Nat Chem Biol. Author manuscript; available in PMC 2016 July 20.

Published in final edited form as:

Nat Chem Biol. 2013 November ; 9(11): 739–745. doi:10.1038/nchembio.1357.

Insights into Mucopolysaccharidosis I from the structure and action of α-L-Iduronidase

Haiying Bie[1,a], **Jiang Yin**[1,a], **Xu He**[2,a], **Allison R. Kermode**[2], **Ethan D. Goddard-Borger**[3], **Stephen G. Withers**[3], and **Michael N. G. James**[1,*]

[1]Department of Biochemistry, University of Alberta, Edmonton, Alberta, Canada, T6G 2H7

[2]Department of Biological Sciences, Simon Fraser University, Burnaby, British Columbia, Canada, V5A 1S6

[3]Department of Chemistry, University of British Columbia, Vancouver, British Columbia, Canada, V6T 1Z1

Abstract

Mucopolysaccharidosis type I (MPS I), caused by mutations in the gene encoding α-L-iduronidase (IDUA), is one of approximately 70 genetic disorders collectively known as the lysosomal storage diseases. To gain insight into the basis for MPS I, we have crystallized human IDUA produced in an *Arabidopsis thaliana cgl* mutant. IDUA consists of a TIM barrel domain containing the catalytic site, a β-sandwich domain and a fibronectin-like domain. Structures of IDUA bound to induronate analogues illustrate the Michaelis complex and reveal a ^{2,5}B conformation in the glycosyl-enzyme intermediate, that suggest a retaining double displacement reaction employing the nucleophilic Glu299 and the general acid/base Glu182. Surprisingly, the N-glycan attached to Asn372 interacts with iduronate analogues in the active site and is required for enzymatic activity. Finally, these IDUA structures and biochemical analysis of the disease-relevant Pro533Arg mutation have enabled us to correlate the effects of mutations in IDUA to clinical phenotypes.

*Correspondence should be addressed to: M.N.G.J., michael.james@ualberta.ca.
[a]These authors have made equal contributions to this paper.

Competing Financial Interests

The authors declare no competing financial interests.

PDB accession codes

Coordinates and structure factors of the R3 and $P2_1$ native crystal forms, 2F-IdoAF, 5F-IdoAF, and IdoA-DNJ complexes have been submitted to the PDB database with their respective accession codes of 4MJ2, 4MJ4, 4KH2, 4KGJ, and 4KGL.

Note: Supplementary information is available in the online version of the paper.

Author Contributions

X.H. and A.R.K. performed the protein production and purification, and the comparative kinetics work related to IDUA deglycosylation and Pro533Arg-IDUA. E.D.G.B. performed chemical synthesis and other enzyme kinetics. H.B. crystallized the protein. H.B. and J.Y. collected the diffraction data and carried out structure determination. H.B., J.Y. and M.N.G.J. analyzed the data and wrote the paper with contributions from X.H., A.R.K., S.G.W. and E.D.G.B.. M.N.G.J. and A.R.K. supervised the project.

Introduction

Lysosomal storage diseases (LSDs) are a broad class of devastating genetic diseases that collectively represent over 70 disorders. Mucopolysaccharidosis type I (MPS I) is an autosomal recessive LSD characterized by a deficiency in the enzyme α-L-iduronidase (IDUA)[1]. IDUA participates in the stepwise degradation of the glycosaminoglycans (GAGs) heparan sulphate and dermatan sulphate, by removing a single α-L-iduronyl residue from the non-reducing ends of these complex polysaccharides. Because of the widespread distribution of GAGs in tissues and organs (in which they typically exist as proteoglycans), severely affected humans with no residual IDUA activity typically die in early childhood because of profound skeletal, cardiac and neurological disturbances[1]. MPS I patients are typically described as belonging to one of three clinical phenotypes: Hurler, Hurler-Scheie, and Scheie, for the severe, intermediate, and attenuated forms of the disease, respectively[2]. MPS I is a rare disease; it is estimated to affect 1 in every 100,000 live births. Collectively, LSDs comprise a significant proportion of childhood metabolic diseases, with a combined frequency of about 1 in every 5,000 live births. The currently approved treatment for MPS I is enzyme replacement therapy (ERT). Due to the high price associated with ERT (~ $450,000 per patient per year) alternative treatments, such as the development of pharmacological chaperones[3–5], are being sought for many of the LSDs.

Over 100 gene mutations causing the various forms of MPS I have been reported[6,7]. Despite the considerable detail available concerning genotypes and the corresponding clinical phenotypes of MPS I, a correlation between the two has been difficult due to the lack of a detailed three-dimensional molecular structure of the enzyme. Not only has the lack of a molecular structure contributed to the difficulty in interpreting the effects of these mutations but also there has been a difficulty in deciphering a detailed enzymatic mechanism for IDUA. The only other member of the family 39 glycoside hydrolases that has had its tertiary structure elucidated is the β-D-xylosidase (TsXy)[8,9] from *Thermoanaerobacterium saccharolyticum*. Those structural analyses contributed to the understanding of a bacterial version of the GH39 family, but the marginal sequence identity between TsXy and the mammalian IDUA (~22% identical)[10] has made it extremely difficult to predict accurately the correct structure of IDUA[11] or to interpret the mechanism of IDUA.

Here we present five comprehensive three-dimensional structures for human IDUA including two apo-enzyme structures and three enzyme-inhibitor complexes. These “snap-shot” structures are instrumental in delineating the full course of catalytic events during substrate hydrolysis by IDUA. A novel finding of a high-mannose N-glycan at Asn372 contributing to the enzymatic activity of IDUA is reported. Taking Pro533Arg, a relatively frequent missense mutation in *IDUA* gene among MPS I patients as a case in point, we discuss the implications of these protein structures for understanding MPS I disease pathophysiology, particularly the enzyme mechanism and some of the phenotype-genotype correlations for predicting clinical phenotypes and the clinical outcomes of ERT. Future design of active-site-specific inhibitors (pharmacological chaperones) as alternative disease therapeutics for MPS I will be greatly aided by our findings.

Results

Crystal Structures of apo-IDUA

The molecular structure of recombinant human IDUA produced in *Arabidopsis thaliana* has been determined in two crystal forms, a rhombohedral form, space group R3 and a monoclinic form, space group $P2_1$ (Supplementary Results, Supplementary Table 1). The R3 crystal form has two molecules in the asymmetric unit and has been refined to 2.1Å resolution; the $P2_1$ crystal form (one molecule/asymmetric unit) has been refined to 2.2Å resolution. Least–squares comparisons among these three molecules show that all three structural determinations agree very well with one another (Supplementary Table 2). As with many of the glycoside hydrolases, IDUA has three prominent domains: a TIM barrel extending from Arg48 to Ala394 (Fig. 1(a)) that contains the active site residues Glu182 and Glu299, a β-sandwich (Glu398 to Ala542) that contains the N-terminus of the enzyme and the first β-strand, β1 (His30 to Leu43) and a third domain (Thr552 to Glu640) that resembles the fold of a type III fibronectin domain and consists of the C-terminal residues of the enzyme (see the topology diagram in Supplementary Fig. 1).

In human IDUA, there are six N-linked glycosylation sites. The oligosaccharide structures at each site of recombinant human IDUA secreted from a Chinese hamster ovary (CHO) cell line have been determined by mass spectrometry[12]. The IDUA expressed in the seeds of a *cgl* mutant of Arabidopsis has much reduced complexity in these N-linked glycans[13], the majority of which are non-matured, high mannose N-glycans (~95%) (Supplementary Note). The two crystal forms that have been determined in the present study reveal only three N-glycosylated Asn residues, Asn110, Asn372 and Asn415. There was no interpretable electron density that could be associated with carbohydrate residues at the other three sites, Asn190, Asn336 and Asn451. The most well defined N-glycan from all of the structures determined is present on Asn372 in the three structures of the IdoA analogues bound to molecule B of IDUA (Supplementary Fig. 2).

There are two unique structural features of IDUA that are found on insertions in a) the TIM barrel domain (β12 and β13) and b) the β-sandwich domain (α15 and α16) (Supplementary Fig. 1). The glycosylation site, Asn372, resides on the β-hairpin insertion between β11 and β14 of the TIM barrel. Asn372 has been shown to be a high mannose site in both forms of recombinant human IDUA (that produced in CHO cells[12] and that produced in plants[13]). Two helices (α15 and α16) are inserted between strands β19 and β20 of the β-sandwich domain. These helices and the loop of polypeptide linking them are packed against the glycan-containing β-hairpin formed by β12 and β13. These two structural features are not observed in the TsXy structure[9].

The third domain of IDUA (extending from Thr552 to the C-terminus of the enzyme) resembles a type III fibronectin fold. The last residue that is visible in our electron density maps is Pro642. The remaining 11 residues are disordered in the present structures (from Val643 to Pro653).

A view of the catalytic residues in the TIM barrel of IDUA is shown in Fig. 1(b). Previous sequence alignments and biochemical studies on the family 39 β-D-xylosidase (TsXy) and

IDUA have provided evidence via LC-mass spectrometric analysis of peptides from labeled enzyme that the nucleophilic carboxylate is Glu299 in IDUA (Glu277 in TsXy) and that the general acid/base in IDUA is Glu182 (Glu160 in TsXy)[8,14]. Subsequently, the crystal structure of a covalently bound 2-deoxy-2-fluoro-α-D-xylosyl-xylosidase intermediate complex confirmed that indeed the nucleophile is Glu277 in TsXy[9]. The relative disposition and surrounding environments of Glu299 and Glu182 in human IDUA are shown in Fig. 1(b). The carboxylates of Glu299 and Glu182 are separated by 5.2Å, a distance that is typically observed in retaining glycoside hydrolases[8,9,15]. The environment of Glu299 is consistent with its carboxyl group being ionized; it is the recipient of two hydrogen bonds, one from N^{ζ} of Lys264 and the other from $N^{\eta 1}$ of Arg89. On the other hand, the carboxyl group of Glu182 is partially buried and does not make hydrogen bonds to other groups on IDUA. It is predicted to have a pKa of 5.6, consistent with a catalytic mechanism that requires it to be protonated at the pH of the lysosome[16].

Structures of IDUA-inhibitor complexes

Through crystal soaking and co-crystallization, we have obtained complexes of IDUA with each of the three substrate analogue/inhibitors, 5-fluoro-α-L-idopyranosyluronic acid fluoride (5F-IdoAF), 2-deoxy-2-fluoro-α-L-idopyranosyluronic acid fluoride (2F-IdoAF), and [2*R*, 3*R*, 4*R*, 5*S*]-2-carboxy-3,4,5-trihydroxy-piperidine (IdoADNJ) (Fig. 2 and Supplementary Table 1). Both 5F-IdoAF and 2F-IdoAF were designed as reagents to trap the glycosyl-enzyme intermediate, though in both cases turnover of this intermediate was seen to be fast[8]. Through flash-cooling of the crystals it was anticipated that either a Michaelis complex or the covalent intermediate might be trapped. IdoADNJ was synthesized as a potential transition state analogue inhibitor, but was found to bind with only weak affinity ($IC_{50} \approx 3$ mM). The refined σ^{A}-weighted, 2||Fo|-|Fc|| electron density maps clearly revealed that both 5F-IdoAF and IdoADNJ are bound in a $^{2}S_{o}$ skew-boat conformation in the active site of IDUA, likely mimicking an enzyme-substrate Michaelis complex on the normal catalytic pathway (Fig. 3(a)). The 2F-IdoAF molecule forms a covalent adduct with the carboxylate group of Glu299 and the resulting 2F-IdoA adduct adopts a distorted $^{2,5}B$ conformation, thereby illuminating the key glycosyl-enzyme intermediate on the catalytic pathway (Fig. 3). The protein structures in all three complexes align very well with one another as well as with the native enzyme structures; r.m.s.d.s range from 0.14 to 0.36Å and there are no detectable inter-domain movements, consistent with these molecular structures representing the catalytically competent conformation of the enzyme (Supplementary Table 2).

In total, the non-covalently bound 5F-IdoAF, forms 11 H-bonds and around 70 van der Waals contacts (cut-off, 4Å) with the enzyme (Fig. 2(a)). 2F-IdoA and IdoADNJ bind to the active site of IDUA with similar numbers of H-bonds and van der Waals interactions (Fig. 2(b)(c)). All of the hydroxyl groups of the IdoA analogues participate in H-bond interactions with IDUA. Furthermore, O3, as seen in molecule B in the asymmetric unit, is involved in a polar interaction with a mannose residue from the oligosaccharide chain extending from the N-glycosylation site Asn372 (Figs. 2, 3(a) and 3(b)).

Role of glycosylation at Asn372

The observation that the N-glycan on Asn372 participates in substrate binding is surprising and to our knowledge, a novel finding for glycosidases. It was previously reported that the major N-glycan on Asn372 of CHO-produced IDUA is of a high-mannose type (Man_9NAG_2)[12]. Similarly, high-mannose structures were found at this position in our plant-produced enzyme[13]. We have traced Man_7NAG_2 in molecule B of the two IDUA molecules in the asymmetric unit of the R3 crystal form. Mannose-D (Man7 in Fig. 3 and Supplementary Fig. 2) which connects to Mannose-B via an α-1,2-linkage, makes polar and van der Waals contacts (< 4Å) with atoms O3, C1, C2, C3, C4 and C5 of the IdoA analogues bound in the active site of IDUA (Figs. 2, 3 (a) and 3(b) and Supplementary Table 3). In addition, this mannose is situated approximately 4.3Å on top of the C5-carboxylate of the IdoA analogues. The active site of IDUA is relatively more open to the solvent compared to that of TsXy; however, it seems that IDUA effectively utilizes this high mannose chain to extend the "back wall" of the IdoA binding pocket upward, thereby separating the bound IdoA from solvent at the α-face. We have determined that the enzymatic activity of the deglycosylated IDUA (IDUA treated with carbohydrate-binding-module-peptide-N-glycosidase F (CBM-PNGase F)) was 11.2% of that of the untreated (glycosylated) IDUA. The K_m and V_{max} of deglycosylated IDUA were roughly 3 times and 50% of the K_m and V_{max} of the untreated IDUA, respectively, suggesting that N-glycosylation is critical for IDUA activity (Fig. 4). Further support of the involvement of Asn372 N-glycan in catalysis came from a report published online while a revised version of this manuscript was being reviewed, that showed a correlation between the level of N-glycosylation at Asn372 and the enzymatic activity of IDUA[17]. A vital role for Asn372 glycosylation in substrate binding or catalysis is a tantalizing prospect; mutation of the N-glycan sequon at position 372 followed by a determination of the kinetic consequences (Km) would be required to assess this thoroughly.

Enzyme-ligand interactions and substrate specificity

Based on kinetics data, a previous study[18] postulated that two cationic binding sites exist in IDUA, one of which might interact with the C5-carboxylate group of IdoA. Evidence for the carboxylate-binding site is now found in our structures. The C5-carboxylates of 5F-IdoAF, 2F-IdoA and IdoADNJ are all bound snugly in a positively charged pocket formed by the side chains of Arg363, and Lys264, and the main chain NH groups of Gly305 and Trp306 of IDUA (Figs. 2(d) and 3(a)(b)). The $N^{\eta 2}$ of Arg363 donates an H-bond of 2.7Å and 2.9Å to one of the carboxylate oxygens (O6A) of 5F-IdoAF in molecules A and B in the asymmetric unit, respectively. This same carboxylate oxygen of 5F-IdoAF also forms H-bonds with the N^{ζ} of Lys264 and the main chain amide nitrogen of Gly305. The other carboxylate oxygen (O6B) of 5F-IdoAF is involved in an H-bond interaction with the main chain nitrogen of Trp306. Such a concentration of H-bonds to the C5-carboxylate suggests that this site may be the anchor point for initial substrate binding. Consistent with this hypothesis, Arg363 is required for IDUA activity in tissue culture (transformed fibroblasts) and an Arg363Cys mutation in IDUA is associated with a clinical manifestation of the Hurler-Scheie (intermediate) MPS I phenotype[19]. Furthermore, the structural recognition of both the presence and proper configuration of the C5-carboxylate of IdoA by IDUA is mutual: an IdoA analogue without the L-configured-C5-carboxylate moiety is not an active substrate for

IDUA[20], indicating an essential role for the specific interactions between IdoA and the carboxylate-binding pocket in substrate recognition and turnover by IDUA.

The O2, O3 and O4 hydroxyl groups of IdoA are also involved in multiple H-bonds with IDUA (Fig. 2). Additionally, F1 and by inference, the glycosidic oxygen atoms of substrate molecules accept an H-bond from the O^{e2} of Glu182. Overall, an extensive network of polar and non-polar interactions exists between these IdoA analogues and IDUA, involving several of the key residues in the active site. The clinical findings that mutations at some of the above residues are associated with MPS I phenotypes also substantiate the importance of these residues in substrate binding and/or catalysis[6].

Implications for the catalytic mechanism

IDUA is an α-retaining glycoside hydrolase with strict substrate specificity for L-IdoA[8]. As shown for many other configuration-retaining glycosidases, the hydrolysis of polysaccharide substrates by IDUA likely proceeds through a double displacement mechanism[21,22]. Our crystal structures have confirmed that the general acid/base in this reaction is Glu182[11]. Furthermore, the covalent complex of IDUA-2F-IdoA is consistent with the general catalytic mechanism of retaining glycosidases[23].

The two key "snapshots" of Ido A analogues bound to IDUA have allowed us to envisage the full course of events along the catalytic pathway (Fig. 3). Fig 3(a) shows a view of an analogue (5F-IdoAF) of the Michaelis complex with the anomeric carbon (C1) of IdoA poised to receive the nucleophilic attack by the carboxylate of Glu299; this ideal spatial placement results from the $^{2}S_{o}$ conformation of the IdoA pyranose ring. The general acid carboxyl group of Glu182 is also ideally positioned to donate a proton to the glycosidic oxygen of a substrate (Fig. 3(d)). In the IDUA-5F-IdoAF complex, the carboxyl group of Glu182 makes an H-bond (3.0Å) to the F1 substituent of the pyranose ring (Fig. 3(a)). The inferred spatial orientation of the general acid and the glycosidic oxygen of a polysaccharide substrate is fully consistent with the lateral protonation mechanism reported for the Clan GHA glycosidases[24].

By superposing the IDUA-5F-IdoAF complex and the IDUA-2F-IdoA adduct, it is possible to appreciate the conformational changes that the pyranose ring undergoes as a result of the electrophilic migration during catalysis[21,22]. The major change is in the position of C1 as it moves ~1.2Å to form the covalent bond to the nucleophilic carboxylate of Glu299 (Fig. 3(c)). As a consequence of this movement through the transition state, the pyranose ring converts from the $^{2}S_{o}$ skew-boat conformation in the Michaelis complex to a $^{2,5}B$ boat conformation in the glycosyl-enzyme intermediate. The equivalent $^{2,5}B$ conformation has been seen previously in the glycosyl-enzyme intermediates of the GH11 family Xylanases with substrates having no C-5 substituents[25,26].

In addition to the conformational changes taking place in the substrate as one traverses the catalytic pathway, there are conformational adjustments in the side chain of Glu299; notably, the χ^{1} angle of Glu299 changes from gauche (−) (−77°) to gauche (+) (54°) conformation (Fig. 3(c)). This results in only a minor difference in the position adopted by the nucleophilic oxygen atom (O^{e1}) and it remains in an ideal orientation to carry out the

nucleophilic attack on the anomeric carbon atom (C1) of the substrate in the Michaelis complex. The N^{ζ} of Lys264 is located about 3.0Å from the ring oxygen in the 2F-IdoA-IDUA complex, a distance suggestive of an H-bond. In the glycosylated intermediate, this potential H-bond would involve one of the lone pair electrons of the ring oxygen in an ideal geometry that can only be satisfied by a $^{2,5}B$ conformation of the IdoA molecule. A similar orientation and distance (~3.0Å) between the endocyclic oxygen of the xylose substrate and the O^{η} of Tyr85 of *Bacillus agaradhaerens* family 11 xylanase was reported previously [25,26].

A water molecule was observed ~3.2Å from the carboxylate of Glu182 and about 4.7Å from the C1 of the covalently attached 2FIdoA molecule (Fig. 2(b)). This is consistent with the role of Glu182 in the second half of the hydrolytic reaction, in which a nucleophilic water molecule, assisted by the general base, Glu182, carries out an in-line attack at the C1 atom to release the second product, iduronic acid from the enzyme.

Correlation of Clinical Phenotypes with IDUA Mutants

More than one hundred mutations in the gene encoding IDUA and that cause disease of variable severity in MPS I patients have been reported[7,19]. Many of these mutations are missense mutations whose structural implications are difficult to predict without a crystal structure of IDUA (Supplementary Fig. 3). Our present structures of human IDUA offer, for the first time, insights into the association between the clinical phenotypes and defects in the IDUA structure caused by the corresponding missense mutations. In Supplementary Table 4 we have listed our analysis of the structural consequences of each mutation. As an initial effort to validate these predictions, we have analyzed the effects of the Pro533Arg mutation on the IDUA structure and enzymatic activity. This is a relatively frequent missense mutation in the IDUA gene that is associated with intermediate to severe MPS I phenotypes and has shown relatively high prevalence in Brazilian, Tunisian and Moroccan MPS I patients[27–30]. Being ~25Å from the catalytic Glu299, Pro533 is located on a loop that connects strands β23 and β24 of the β-sandwich domain; this loop interacts with helix α13 of the TIM barrel and with a helical loop leading to α15. Through a core of hydrophobic interactions with β23, β24 and α16, helix α15 is intimately involved in positioning the N-glycan chain on Asn372 that lies above the active site of IDUA and makes contact with the substrate (Supplementary Fig. 1 and Fig. 5(a)(b)). Pro533 is surrounded by the side chains of Ala448, Leu535, and Val316 (Fig. 5(c)); replacement of the proline by the much bulkier and positively charged arginine at position 533 is likely to cause serious structural perturbations due to both space limitation and to the charge on the arginine residue. By affecting the conformation of the TIM barrel as well as the position of α15 hence the conformation of the Asn372-linked N-glycan, the Pro533Arg mutation may impair catalysis, and possibly also the ability of IDUA to bind its natural substrates. Such a structural perturbation could also affect protein folding, interfering with the ability of the IDUA enzyme to pass ER quality control, and thus undergo maturation and trafficking to the lysosome, as intimated by a previous report[27]. In further examining the effects of this mutation on IDUA activity by *in vitro* assays performed on the purified recombinant enzymes, the K_m of the Pro533Arg IDUA mutant for the artificial (4MUI) substrate was relatively unaffected, whereas the V_{max} decreased by two-fold when compared to that of the wild type enzyme (Fig. 5(d)). Furthermore, heat inactivation experiments indicated that the Pro533Arg mutant has a lower

thermodynamic stability as compared to the wild-type enzyme (Fig. 5(e)). This largely supports the data in two previous reports [27,31] and the conclusions therein regarding the Pro533Arg IDUA mutant as not only having lowered specific activity, but also showing significant impairment in processing/trafficking.

Discussion

MPS I, like many other LSDs, is associated with varying degrees of clinical severity and significant symptom heterogeneity in patients who may carry one or two types of debilitating mutations in the IDUA alleles. The only current FDA-approved therapy for MPS I is ERT; this type of therapy has drawbacks in both efficacy and cost. Our crystal structures of IDUA provide the first glimpse into the molecular organization of the enzyme's active site in both the apo- and the ligand-bound conformations. Such structural information has substantially enhanced our understanding of the catalytic mechanism of IDUA and related enzymes involved in a family of important human disorders. While our structural models cannot directly predict how mutations will affect the rates of IDUA protein folding, or the *in situ* half-life of IDUA in different human tissues, they nonetheless provide an extremely valuable basis for casting viable predictions that can later be tested. It will be imperative to follow up this work with a detailed characterization of how the various missense mutations directly affect the catalytic ability of the IDUA enzyme, and/or impede the maturation pathway leading to the functional IDUA enzyme within the lysosome. Our findings provide a solid basis for clinical prognosis of outcomes of ERT and for future structure-based drug design and synthesis aimed at developing alternative MPS I therapeutics via the "pharmacological chaperone" approach.

Online Methods

Synthesized IDUA inhibitors

2*R*,3*R*,4*R*,5*S*-Trihydroxypipecolic acid (NDJ-IdoA, nojirimycin) was prepared according to the procedure previously reported[32]. ^{1}H and ^{13}C NMR spectra of this material were in agreement with previously reported data[32]. 2-Deoxy-2-fluoro-α-L-iduronyl fluoride (2F-IdoAF) and 5-Fluoro-α-L-iduronyl fluoride (5F-IdoAF) were prepared according to the procedures reported previously[8]. ^{1}H and ^{13}C NMR spectra of these two compounds were in agreement with previously reported data[8].

Transgenic *Arabidopsis cgl* seeds and affinity purification of recombinant human IDUA

Arabidopsis cgl Line A4.7 (described in Supplementary Note) was used in the present study, in which the T2 generation seeds are characterized by IDUA activity of 745 ± 75 units/mg TSP (total soluble protein) and IDUA protein 1.7% TSP or 2.7 μg/mg dry seeds[33]. The IDUA yield was further improved by selfing of plants and further selection. Briefly, T2 seeds from line A4.7 were germinated on selection media (25 mg/L kanamycin in half-strength Murashige and Skoog [MS] medium)[13,33]. Ten to fifteen transgenic seedlings from each line were grown to maturity and selfed to obtain T3 seeds. Protein was extracted from each seed stock and the expression levels determined by activity assays and western blot

analyses (data not shown). In the T3 seeds the recombinant IDUA reached 7.2 ± 0.6 % total soluble protein (9.8 μg/mg dry seeds).

Human recombinant IDUA was purified to homogeneity from the T3 seeds using concanavalin A-sepharose- and anti-IDUA affinity chromatography as described previously[34,35].

Crystallization

Prior to crystallization trials, IDUA was further purified by HiLoad 16/60 Superdex 75 size-exclusion chromatography column to remove any impurities; it was then concentrated to 10 mg/ml for crystallization. The IDUA protein was crystallized using the sitting-drop vapor diffusion method. Two distinct morphologies of crystals were observed after 5–7 days growth at room temperature. The best-isolated needle-shaped crystals were grown from condition 84 of the Index Screen (0.2M $MgCl_2$, 0.1M HEPES pH 7.5, 25% PEG 3350, Hampton Research, Aliso Viejo, CA) together with semi-crystalline spherulites also reported previously[36]. The rhomboid plate-shaped crystals were grown from condition 86 of the Index Screen (0.2M sodium potassium tartrate, 20% PEG 3350, Hampton Research, Aliso Viejo, CA). The crystals were further optimized by vapor diffusion in a hanging-drop tray and the best rhomboid-plate-shaped crystals resulted from solutions of 0.01M HEPES pH 7.5, 0.26M sodium potassium tartrate, and 20% PEG 3350 at room temperature.

Initially we tried to solve the IDUA structure by molecular replacement method using several different search models: TsXy (1PX8)[9], which shares the highest sequence identity of 22% (101/465) with IDUA, and the homology model of IDUA[8], but no definitive solution was obtained. Subsequently, we carried out a number of heavy-atom-derivative screening trials using Heavy Atom Screen (Pt, Hg, Au, and M2) from Hampton Research (Aliso Viejo, CA). We prepared a number of native rhomboid-plate-shaped crystals and soaked them with different heavy atoms at 2mM and at 5mM concentrations. The ethyl-mercuric phosphate (EMP) and K_2PtCl_4 soaked crystals produced fluorescence signals, but the soaking procedure tended to damage the crystals and the diffraction spots were smeared out. In order to obtain high-quality heavy-atom diffraction data containing a strong anomalous signal, we prepared the co-crystals of IDUA in the presence of 2 mM and 5 mM Pt and Hg compounds. The crystal structure was ultimately solved by SAD phasing, using the data collected from a co-crystal of IDUA grown in 5mM EMP.

The 2F-IdoA- and 5F-IdoAF-IDUA complexes were obtained by soaking native R3 crystals into 20 mM concentration of inhibitors for 15 min and 25 min, respectively. To grow IdoADNJ-IDUA complex, the 5 mM inhibitor IdoADNJ was added to the protein solution and incubated at room temperature for 30 min before setting up the crystallization trays. The IdoADNJ-IDUA cocrystals were grown at the same condition as the native R3 crystal. All crystals were cryoprotected in mother liquor containing 30% glycerol and then flash cooled in liquid nitrogen.

Data collection

X-ray diffraction data of all native crystals were collected on beam lines 08B1 and 08ID at the Canadian Light Source, and the datasets of three inhibitor-IDUA complexes were

collected on beamline 11-1 at the Stanford Synchrotron Radiation Lightsource. The R3 Hg-derivative SAD dataset was collected at the Hg peak energy of 1.0064Å. We collected 1000 frames with an oscillation angle of 1.2° per image and a crystal-to-detector distance of 400 mm to produce a high-redundancy dataset for the SAD phasing. The R3 native dataset was collected with a crystal-to-detector distance of 320 mm and a wavelength of 0.9793Å. We collected 360 frames with an oscillation angle of 1°. The $P2_1$ native dataset was collected using a Mar325 detector on beamline 08ID with a crystal-to-detector distance of 300mm and an oscillation angle of 0.5° per frame (covering a total oscillation range of 180°). Three inhibitor-IDUA complexes datasets were collected at a wavelength of 0.97945Å and 180 images were collected with an oscillation angle of 1°.

The raw data of R3 native, R3 Hg-SAD, and 5F-IdoAF-IDUA complex were indexed, integrated, and scaled with the XDS suite of programs[37], and the data of native $P2_1$, 2F-IdoAF-IDUA, and IdoA-DNJ-IDUA complexes were processed with HKL-2000[38].

Structure solution and refinement

The heavy-atom coordinates, phases and density modification map were calculated by *autosol* of the Phenix program suite[39]. Four distinct Hg atoms were observed per asymmetric unit. The resultant phasing figure of merit was 0.27. After the density modification, the resulting high-quality electron density map was used for the model-building with *ARP/wARP*[40]. After *ARP/wARP*, 90% of the amino-acid residues were in density and the remaining amino acids and the carbohydrate residues were manually built using the program Coot[41] and refined with the program REFMAC5[42,43]. The correct side chain orientations of His, Asn, and Gln have been checked by REDUCE[44]. The high resolution $P2_1$ native structure was solved by molecular replacement using the program Phaser[45] and the R3 structure solution as the search model. TLS refinement[46] was performed using 12 TLS groups determined by the TLS Motion Determination (TLSMD) server[47]. The stereochemical quality of the protein model was checked using PROCHECK[48]. In the $P2_1$ crystal form, 99.4% of the residues were in the favored regions of the Ramachandran plot without any outliers. In the R3 crystal form, 99.4% of the residues were in favored regions of the Ramachandran plot with 0.4% outliers.

Deglycosylation of *cgl*-IDUA and effect of deglycosylation on enzyme activity

Approximately 3 mg of purified *cgl*-IDUA was deglycosylated by incubating the *cgl*-IDUA with 30 μg CBM-PNGase F in a buffer containing 20 mM Tris (pH 7.0) and 0.5 M NaCl at 22 °C overnight. The resultant protein mixture was fractionated and checked by 10% SDS-PAGE to ensure complete deglycosylation (data not shown). Removal of the CBM-PNGase F was achieved by applying the protein mixture to a 50 mg Avicel slurry. The great majority of *cgl*-IDUA molecules possess N-glycans that are in a high mannose form[35]; these are removed by CBM-PNGase F. A small fraction of *cgl*-IDUA molecules, however possess complex N-glycans containing α-1,3-fucose residues (~4.2%)[35]. This small fraction of *cgl*-IDUA molecules is resistant to deglycosylation by CBM-PNGase F, and was removed from the high mannose form using Con A Sepharose chromatography. Enzyme activities of *cgl*-IDUA and deglycosylated *cgl*-IDUA were determined in triplicate using an *in vitro* assay in which 1 mM of the substrate (4-methylumbelliferyl α-L-idopyranosid)uronic acid and 0.02

μg of the IDUA enzymes were incubated at 37 °C for 10 min in a total volume of 15 μL containing 0.1 M dimethylglutarate buffer pH 4.5, 2 mM sodium metabisulfite and 0.35% bovine serum albumin, as described previously[13]. For a description of the effect of IDUA deglycosylation on kinetics, see subsequent methods section entitled "Determination of enzyme kinetic parameters of IDUA".

Expression of recombinant human (wild-type) IDUA and Pro533Arg-IDUA genes in tobacco BY-2 cells and purification of the recombinant proteins

The Pro533Arg mutation was engineered into the cDNA encoding the wild-type (WT) human IDUA (GenBank accession no. M74715) using the Quick Change site-directed mutagenesis kit (Stratagene, Santa Clara, USA). The primers used for mutagenesis were: 5′-CGCTGCGGCTGCGGTCGCTTTTGCT-3′ (forward) and 5′-AGCAAAAGCGACCGCAGCCGCAGCG-3′ (reverse). To allow for efficient synthesis and secretion of the recombinant IDUA proteins, a sequence encoding the signal peptide of proaleurain (MAHARVLLLALAVLATAAVAVA) was used to replace the sequence encoding the signal peptide of human IDUA using the following primers: 5′-CTCGCCGTCCTGGCCACGGCCGCCGTCGCCGTCGCCGAGGCCCCGCACCTGGTG CAGGTG (SPp-IDUA-F1), 5′-CACCATGGCCCACGCCCGCGTCCTCCTCCTGGCGCTCGCCGTCCT GGCCACGGCCG (SPp-IDUA-F2), and 5′-TCATGGATTGCCCGGGGATGG (IDUA-R). The PCR products were cloned into a Gateway entry vector pENTR/D-TOPO (Invitrogen, Burlington, Canada) and the DNA sequences were determined. The resulting constructs containing sequences encoding the WT and Pro533Arg IDUA were sub-cloned into a Gateway expression vector (pSITE-0B)[49], which carries the neomycin phosphotransferase II gene (for kanamycin resistance) and the cauliflower mosaic virus (CaMV) 35S promoter (with a duplicated enhancer element; 2X35S) to drive expression of the WT and mutant IDUA genes.

Transformation of tobacco BY-2 cells was carried out as described previously.[50]. After screening the resulting cell lines by IDUA activity assays and western blot analysis, two stable high-expressing lines for WT and Pro533Arg-IDUA were identified for IDUA protein purification. For this, the BY-2 cells expressing WT-IDUA or P533R-IDUA were ground in liquid nitrogen with a mortar and pestle. The powder was then extracted in buffer A (20 mM Tris, pH 7.0, 0.5 M NaCl, 0.5 mM PMSF and 0.02% sodium azide). After centrifugation for 20 min at 3500 rpm, the supernatant was passed through three layers of Miracloth (EMD Biosciences, Inc. La Jolla, CA, USA) and centrifuged at 30,000 rpm at 4 °C for 45 min in an ultracentrifuge (Beckman Coulter Optima L-100 K). The supernatant was loaded onto a column containing Affi-Gel-bound to monoclonal anti-IDUA at 10 ml/h for overnight (recycling) at 4 °C. After washing the unbound protein with buffer A, the IDUA was eluted with buffer B (50 mM sodium citrate, pH 4.0, 2 M NaCl, 0.02% sodium azide) and the eluate was concentrated with Amicon 30 kDa centrifuge filters. Protein concentrations were determined using the Bio-Rad DC™ (Bio-Rad Laboratories, Mississauga, Canada) protein assay kit and bovine serum albumin as standard. Enzyme kinetic parameters of WT IDUA and Pro533Arg IDUA were determined using methods noted in the section below.

Determination of enzyme kinetic parameters of IDUA

IDUA was purified to homogeneity as indicated by SDS-PAGE analysis. Michaelis-Menten kinetics for plant-derived IDUA were determined at 37 °C and pH 4.5 using a fluorometric assay as described previously[35]. Reactions were performed in a total volume of 100 μL, with ~35 ng of purified plant-derived IDUA in a buffer containing 0.1 M dimethylglutarate (pH 4.5), 2 mM sodium metabisulfite and 0.35% bovine serum albumin and substrate (4-Methylumbelliferyl α-L-idopyranosid)uronic acid (Cat. No. M334701, Toronto Research Chemicals, Toronto, Ontario, Canada) (at concentrations of 1–750 μM). All measurements were made in triplicate. Rates of reaction were determined by dividing by the reaction time and concentration of the enzyme, and fit to a Michaelis-Menten curve using GraphPad Prism version 6.01 for Windows (GraphPad Software, La Jolla, California, USA, www.graphpad.com).

Heat inactivation

Equal amounts of the purified Pro533Arg and wild-type enzymes were incubated at 50 °C in the storage buffer (20 mM dimethylglutaric acid, pH 6.0, 0.2 M NaCl, 5% (v/v) glycerol, 5% (v/v) ethonaol) and their catalytic activities on the synthetic substrate 4-MUI were monitored over time. Enzyme activity assay condition is the same as described above using 4-MUI (Toronto Research Chemicals, Toronto, Ontario, Canada) at 750 μM. For each enzyme, three replicates were taken at each time point and chilled on ice followed by determination of enzyme activities. Residual activity was taken as the percentage of enzyme activity at time zero. Data were plotted as mean ± s.d.. To evaluate the decrease of residual enzymatic activity of the Pro533Arg mutant IDUA relative to that of the wild-type IDUA enzyme, simultaneous multiple comparison of the measurements at all time points except for time zero was performed using the Bonferonni correction (R package version 3.0.0, www.r-project.org). The significance level α for the overall comparison was set to be 0.05 and the null hypothesis of no difference between the Pro533Arg and wild-type IDUA was strongly rejected.

Supplementary Material

Refer to Web version on PubMed Central for supplementary material.

Acknowledgments

This paper is dedicated to the memory of John Colter (1923–2013), chair of the Department of Biochemistry, University of Alberta from 1961 to 1987. We thank Sheraz Khan for his technical assistance during in-house data collection and the staff at the Canadian Light Source in Saskatoon and the Stanford Synchrotron Radiation Lightsource for their assistance in the data collection. We are grateful for the initial work done by Katherine Bateman on the growth of the monoclinic form of IDUA crystals, for synthetic work performed by Dr. Alexander Wong, and for the expression and purification of CBM-PNGase-F by Emily Kwan. We also thank J. Hopwood for the monoclonal antibody to human IDUA. M.N.G.J. and A.R.K. are grateful for the funding support from the Canadian Institutes for Health Research (Grant # MOP123222). H.B. thanks Alberta Innovates Health Solution for the fellowship support. E.D.G.B thanks the Canadian Institute of Health Research for a postdoctoral fellowship. A.R.K. is grateful for the funding support from the Canadian Society for Mucopolysaccharide and Related Diseases (Canadian MPS Society) and to the Michael Smith Foundation for Health Research for the Senior Scholar Award (Award number: CI-SSH-01915(07-1)).

References

1. Clarke LA. The mucopolysaccharidoses: a success of molecular medicine. Expert Rev Mol Med. 2008; 10:e1. [PubMed: 18201392]
2. Roubicek M, Gehler J, Spranger J. The clinical spectrum of alpha-L-iduronidase deficiency. Am J Med Genet. 1985; 20:471–81. [PubMed: 3922223]
3. Valenzano KJ, et al. Identification and characterization of pharmacological chaperones to correct enzyme deficiencies in lysosomal storage disorders. Assay Drug Dev Technol. 2011; 9:213–35. [PubMed: 21612550]
4. Tropak MB, et al. Identification of pharmacological chaperones for Gaucher disease and characterization of their effects on beta-glucocerebrosidase by hydrogen/deuterium exchange mass spectrometry. Chembiochem. 2008; 9:2650–62. [PubMed: 18972510]
5. Yu Z, Sawkar AR, Kelly JW. Pharmacologic chaperoning as a strategy to treat Gaucher disease. FEBS J. 2007; 274:4944–50. [PubMed: 17894779]
6. Neufeld, EF., Muenzer, J. The mucopolysaccharidoses. In: Scriver, CR., et al., editors. The Metabolic and Molecular Bases of Inherited Disease. Vol. III. McGraw-Hill; New York: 2001.
7. Terlato NJ, Cox GF. Can mucopolysaccharidosis type I disease severity be predicted based on a patient's genotype? A comprehensive review of the literature. Genet Med. 2003; 5:286–94. [PubMed: 12865757]
8. Nieman CE, et al. Family 39 alpha-l-iduronidases and beta-D-xylosidases react through similar glycosyl-enzyme intermediates: identification of the human iduronidase nucleophile. Biochemistry. 2003; 42:8054–65. [PubMed: 12834357]
9. Yang JK, et al. Crystal structure of beta-D-xylosidase from Thermoanaerobacterium saccharolyticum, a family 39 glycoside hydrolase. J Mol Biol. 2004; 335:155–65. [PubMed: 14659747]
10. Altschul SF, Gish W, Miller W, Myers EW, Lipman DJ. Basic local alignment search tool. J Mol Biol. 1990; 215:403–10. [PubMed: 2231712]
11. Rempel BP, Clarke LA, Withers SG. A homology model for human alpha-l-iduronidase: insights into human disease. Mol Genet Metab. 2005; 85:28–37. [PubMed: 15862278]
12. Zhao KW, Faull KF, Kakkis ED, Neufeld EF. Carbohydrate structures of recombinant human alpha-L-iduronidase secreted by Chinese hamster ovary cells. J Biol Chem. 1997; 272:22758–65. [PubMed: 9278435]
13. He X, et al. Characterization and downstream mannose phosphorylation of human recombinant alpha-L-iduronidase produced in Arabidopsis complex glycan-deficient (cgl) seeds. Plant Biotechnol J. 2013
14. Vocadlo DJ, MacKenzie LF, He S, Zeikus GJ, Withers SG. Identification of glu-277 as the catalytic nucleophile of Thermoanaerobacterium saccharolyticum beta-xylosidase using electrospray MS. Biochem J. 1998; 335(Pt 2):449–55. [PubMed: 9761746]
15. Armand S, et al. Stereochemical course and reaction products of the action of beta-xylosidase from Thermoanaerobacterium saccharolyticum strain B6A-RI. Eur J Biochem. 1996; 236:706–13. [PubMed: 8612648]
16. Rostkowski M, Olsson MH, Sondergaard CR, Jensen JH. Graphical analysis of pH-dependent properties of proteins predicted using PROPKA. BMC Struct Biol. 2011; 11:6. [PubMed: 21269479]
17. Maita N, et al. Human alpha-L-iduronidase uses its own N-glycan as a substrate-binding and catalytic module. Proc Natl Acad Sci U S A. 2013
18. Hopwood JJ, Muller V. Diagnostic Enzymology of a-L-Iduronidase with Special Reference to a Sulfated Disaccharide Derived from Heparin. Clin Sci (Lond). 1982; 62:193–201. [PubMed: 6895615]
19. Yogalingam G, et al. Identification and molecular characterization of alpha-L-iduronidase mutations present in mucopolysaccharidosis type I patients undergoing enzyme replacement therapy. Hum Mutat. 2004; 24:199–207. [PubMed: 15300847]
20. Clements PR, Muller V, Hopwood JJ. Human alpha-L-iduronidase. 2. Catalytic properties. Eur J Biochem. 1985; 152:29–34. [PubMed: 4043083]

21. Vocadlo DJ, Davies GJ, Laine R, Withers SG. Catalysis by hen egg-white lysozyme proceeds via a covalent intermediate. Nature. 2001; 412:835–8. [PubMed: 11518970]
22. Davies GJ, Planas A, Rovira C. Conformational analyses of the reaction coordinate of glycosidases. Acc Chem Res. 2012; 45:308–16. [PubMed: 21923088]
23. Koshland DE. Stereochemistry and the Mechanism of Enzymatic Reactions. Biol Rev Camb Philos Soc. 1953; 28:416–436.
24. Heightman TD, Vasella AT. Recent insights into inhibition, structure, and mechanism of configuration-retaining glycosidases. Angew Chem Int Ed Engl. 1999; 38:750–770.
25. Sabini E, et al. Catalysis and specificity in enzymatic glycoside hydrolysis: a 2,5B conformation for the glycosyl-enzyme intermediate revealed by the structure of the Bacillus agaradhaerens family 11 xylanase. Chem Biol. 1999; 6:483–92. [PubMed: 10381409]
26. Sidhu G, et al. Sugar ring distortion in the glycosyl-enzyme intermediate of a family G/11 xylanase. Biochemistry. 1999; 38:5346–54. [PubMed: 10220321]
27. Matte U, et al. Identification and characterization of 13 new mutations in mucopolysaccharidosis type I patients. Mol Genet Metab. 2003; 78:37–43. [PubMed: 12559846]
28. Alif N, et al. Mucopolysaccharidosis type I: characterization of a common mutation that causes Hurler syndrome in Moroccan subjects. Ann Hum Genet. 1999; 63:9–16. [PubMed: 10738517]
29. Laradi S, et al. Mucopolysaccharidosis I: Alpha-L-Iduronidase mutations in three Tunisian families. J Inherit Metab Dis. 2005; 28:1019–26. [PubMed: 16435195]
30. Scott HS, et al. alpha-L-iduronidase mutations (Q70X and P533R) associate with a severe Hurler phenotype. Hum Mutat. 1992; 1:333–9. [PubMed: 1301941]
31. Bunge S, et al. Genotype-phenotype correlations in mucopolysaccharidosis type I using enzyme kinetics, immunoquantification and in vitro turnover studies. Biochim Biophys Acta. 1998; 1407:249–56. [PubMed: 9748610]
32. Bashyal BP, Chow HF, Fellows LE, Fleet GWJ. The synthesis of polyhydroxylated amino acids from glucuronolactone: enantiospecific synthesis of 2*S*,3*R*,4*R*,5*S*-trihydroxypipecolic acid, 2*R*,3*R*,4*R*,5*S*-trihydroxypipecolic acid and 2*R*,3*R*,4*R*-dihydroxyproline. Tetrahedron. 1987; 43:415–422.
33. Downing WL, et al. Synthesis of enzymatically active human alpha-L-iduronidase in Arabidopsis cgl (complex glycan-deficient) seeds. Plant Biotechnol J. 2006; 4:169–81. [PubMed: 17177794]
34. He X, et al. Production of alpha-L-iduronidase in maize for the potential treatment of a human lysosomal storage disease. Nat Commun. 2012; 3:1062. [PubMed: 22990858]
35. He X, et al. Influence of an ER-retention signal on the N-glycosylation of recombinant human alpha-L-iduronidase generated in seeds of Arabidopsis. Plant Mol Biol. 2012; 79:157–69. [PubMed: 22442036]
36. Ruth L, Eisenberg D, Neufeld EF. alpha-L-iduronidase forms semi-crystalline spherulites with amyloid-like properties. Acta Crystallogr D Biol Crystallogr. 2000; 56:524–8. [PubMed: 10739940]
37. Kabsch W. Xds. Acta Crystallogr D Biol Crystallogr. 2010; 66:125–32. [PubMed: 20124692]
38. Otwinowski Z, Minor W. Processing of X-ray Diffraction Data Collected in Oscillation mode. Methods Enzymol. 1997; 276:307–326.
39. Adams PD, et al. PHENIX: a comprehensive Python-based system for macromolecular structure solution. Acta Crystallogr D Biol Crystallogr. 2010; 66:213–21. [PubMed: 20124702]
40. Langer G, Cohen SX, Lamzin VS, Perrakis A. Automated macromolecular model building for X-ray crystallography using ARP/wARP version 7. Nat Protoc. 2008; 3:1171–9. [PubMed: 18600222]
41. Emsley P, Cowtan K. Coot: model-building tools for molecular graphics. Acta Crystallogr D Biol Crystallogr. 2004; 60:2126–32. [PubMed: 15572765]
42. Winn MD, et al. Overview of the CCP4 suite and current developments. Acta Crystallogr D Biol Crystallogr. 2011; 67:235–42. [PubMed: 21460441]
43. Murshudov GN, et al. REFMAC5 for the refinement of macromolecular crystal structures. Acta Crystallogr D Biol Crystallogr. 2011; 67:355–67. [PubMed: 21460454]

44. Word JM, Lovell SC, Richardson JS, Richardson DC. Asparagine and glutamine: using hydrogen atom contacts in the choice of side-chain amide orientation. J Mol Biol. 1999; 285:1735–47. [PubMed: 9917408]
45. McCoy AJ, et al. Phaser crystallographic software. J Appl Crystallogr. 2007; 40:658–674. [PubMed: 19461840]
46. Winn MD, Murshudov GN, Papiz MZ. Macromolecular TLS refinement in REFMAC at moderate resolutions. Methods Enzymol. 2003; 374:300–21. [PubMed: 14696379]
47. Painter J, Merritt EA. Optimal description of a protein structure in terms of multiple groups undergoing TLS motion. Acta Crystallogr D Biol Crystallogr. 2006; 62:439–50. [PubMed: 16552146]
48. Laskowski RA, Macarthur MW, Moss DS, Thornton JM. PROCHECK: a program to check the stereochemical quality of protein structures. J Appl Crystallogr. 1993; 26:283–291.
49. Chakrabarty R, et al. PSITE vectors for stable integration or transient expression of autofluorescent protein fusions in plants: probing Nicotiana benthamiana-virus interactions. Mol Plant Microbe In. 2007; 20:740–50.
50. Babajani G, Tropak MB, Mahuran DJ, Kermode AR. Pharmacological chaperones facilitate the post-ER transport of recombinant N370S mutant beta-glucocerebrosidase in plant cells: evidence that N370S is a folding mutant. Mol Genet Metab. 2012; 106:323–9. [PubMed: 22592100]

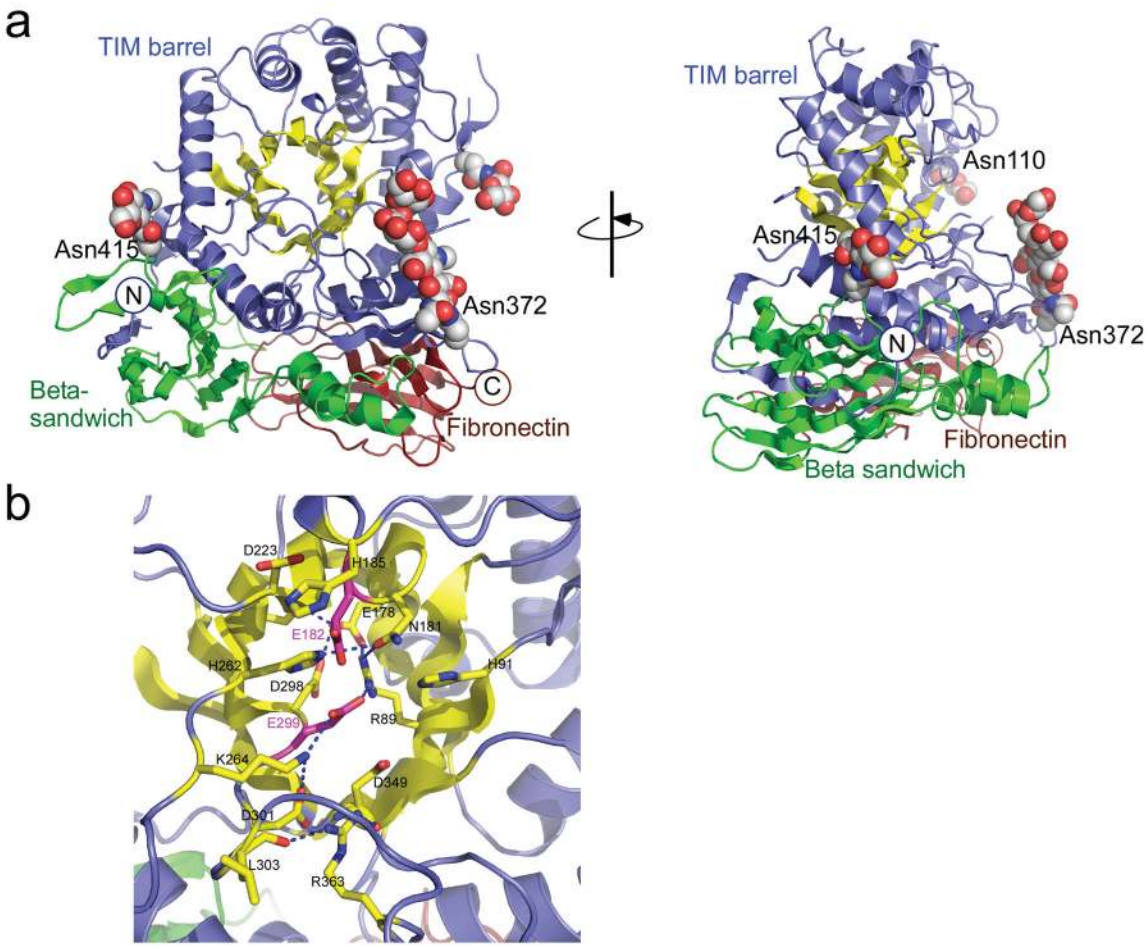

Figure 1. Overview of the IDUA molecule and close-up view of the catalytic domain

(a) Two views (related by a 90° rotation) of the complete apo-IDUA molecule from the $P2_1$ crystal form. The TIM barrel is colored slate blue with the central eight strands of the β–barrel represented in yellow. Three of the six possible N-glycosylation sites have electron density for the attached sugar residues; Asn110 has a single NAG; Asn372 has five saccharide residues (Man_3NAG_2) and Asn415 has a single NAG (Supplementary Fig. 2). The β-sandwich domain is represented in green. The C-terminal type III fibronectin-like domain is represented in a red color. **(b)** A close-up view of the active site of IDUA. The carbon atoms of the nucleophile, Glu299 and the general acid/base, Glu182 are colored in magenta. Other residues that are proposed to be of importance in substrate binding and the catalytic mechanism are colored in yellow for the carbon atoms, red for oxygen atoms and blue for nitrogen atoms. The residues involved in substrate binding are: Arg363, Asp349, His91 and Asn181. Arg89 and Lys264 provide a positively-charged environment that ensures a depressed pK_a for the carboxyl group of Glu 299.

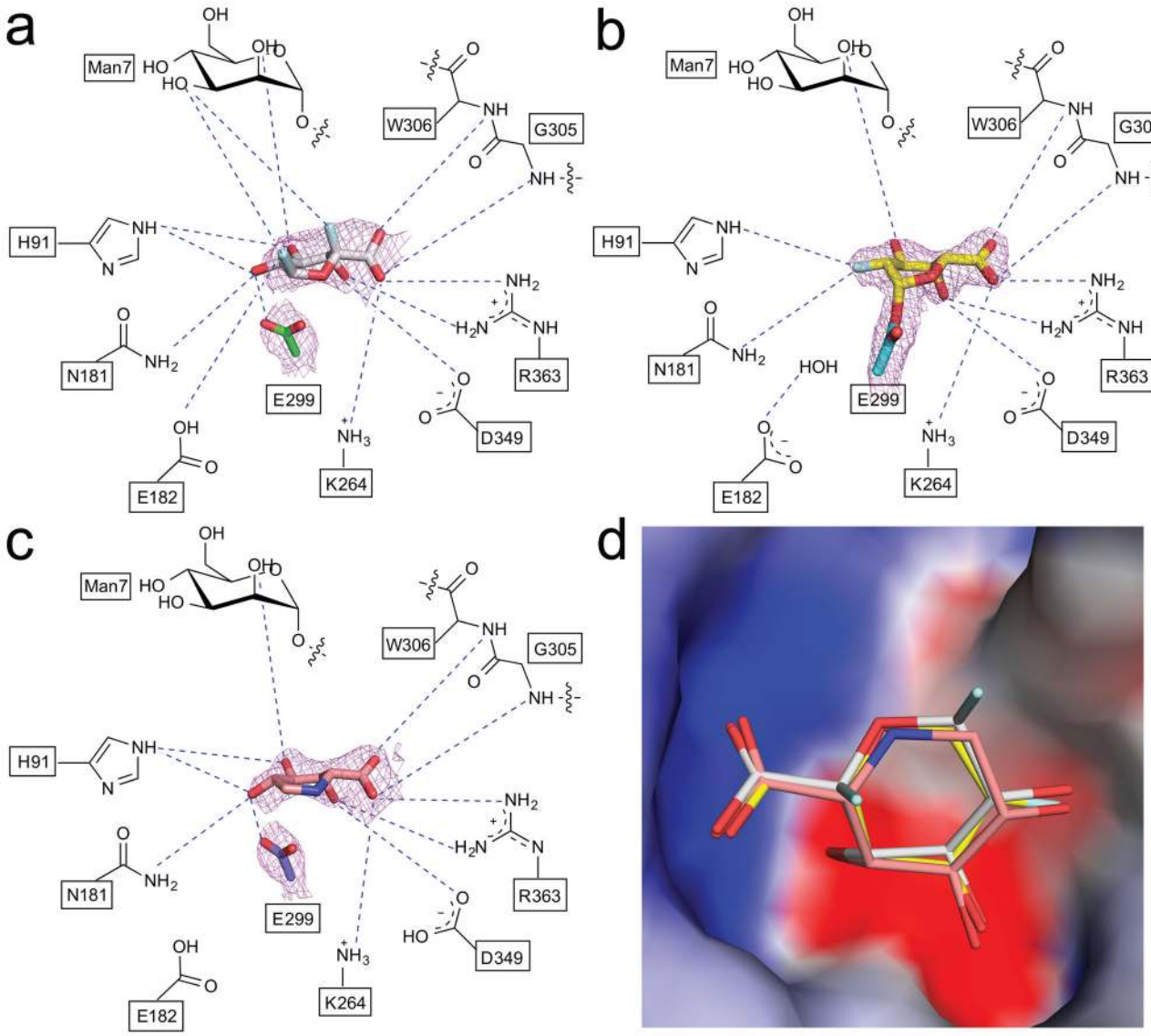

Figure 2. Schematic views of the polar interactions between IdoA analogues and IDUA

(a) The interactions between 5F-IdoAF and IDUA; **(b)** the interactions between 2F-IdoA and IDUA; **(c)** the interactions between IdoADNJ and IDUA; **(d)** the electrostatic potential surface representation of the IDUA active site, blue and red indicate positive and negative potentials, respectively. The ligands and the nucleophile Glu299 are shown in the conformations observed in the crystal structures with the surrounding σ^A-weighted $2||F_o|-|F_c||$ electron density contoured at 1 σ shown in violet-purple mesh.

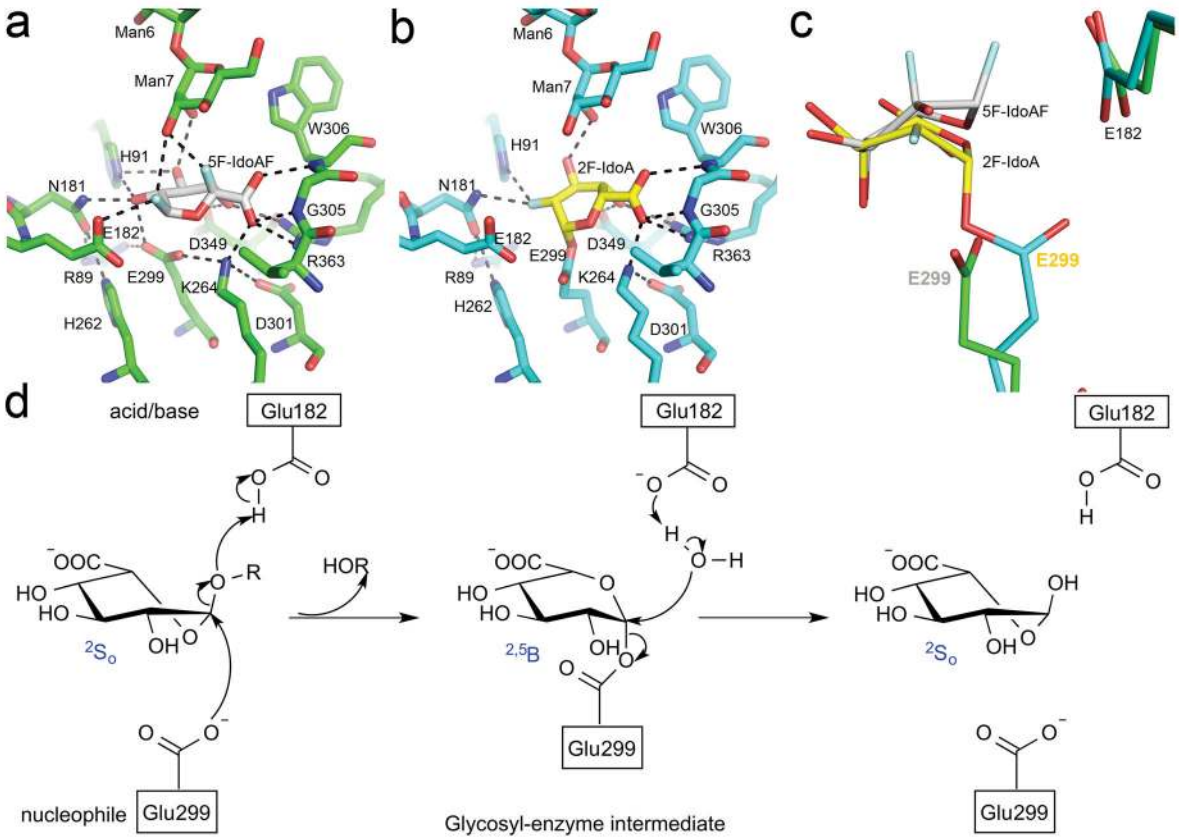

Figure 3. The catalytic pathway for human IDUA and supporting crystallographic evidence

a) A model of the Michaelis complex with 5F-IdoAF bound in the active site of IDUA. The enzyme residues are distinguished by carbon atoms highlighted in green, whereas the ligand carbon atoms in grey. Hydrogen bonds are represented by dashed lines. **(b)** The glycosyl-enzyme intermediate as seen in the active site of IDUA with Glu299 covalently modified by 2F-IdoAF. The carbon atoms of the enzyme residues are highlighted in cyan, while those of the ligand are shown in yellow. **(c)** A comparative "front" view of the 5F-IdoAF and covalently bound 2F-IdoA in the active site of IDUA, the C2-C5 axis of the IdoA ring runs almost perpendicular to the plane of the paper. The anomeric carbon "travels" ~1.2Å downward from its position in the IDUA-5F-IdoAF complex to that in the IDUA-2F-IdoA adduct. **(d)** The proposed catalytic pathway of IDUA. See text for details. Note that acid catalysis by Glu 182 may not be important for fluoride departure but is crucial for the natural substrate of IDUA.

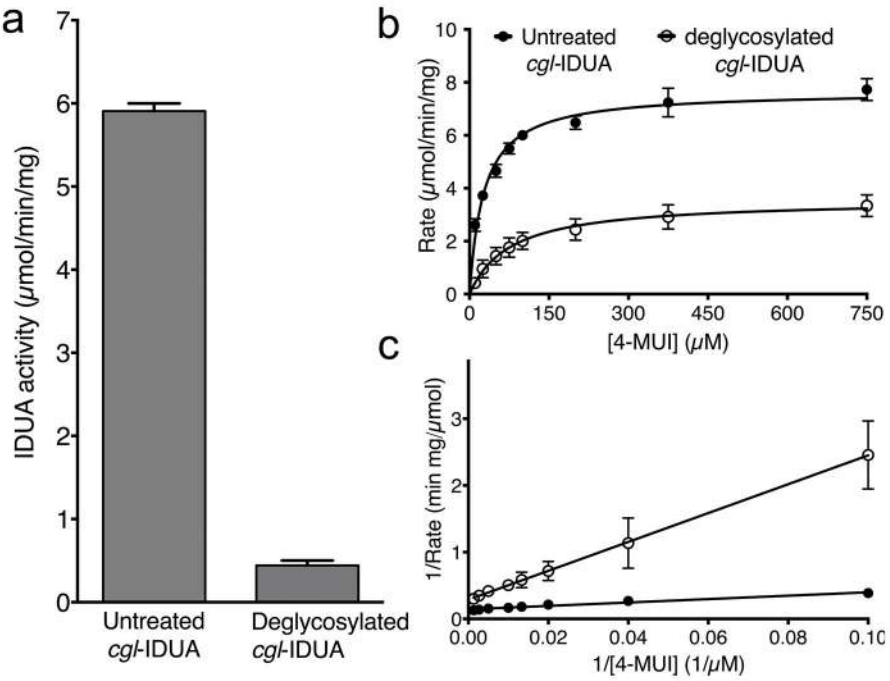

Figure 4. Marked effects of deglycosylation by CBM-PNGase F on the hydrolytic activity of *cgl*-IDUA and kinetic parameters

(a) Almost 10-fold reduction in enzymatic activities after deglycosylation of *cgl*-IDUA by CBM-PNGase F. **(b)** Michaelis-Menten and **(c)** Lineweaver-Burk plots of the reaction rates vs. concentration of the fluorescent substrate (4-methylumbelliferyl α-L-idopyranosid)uronic acid (4-MUI). All assays were carried out in triplicate and the results are presented as mean ± s.d.. The kinetic values, K_m and V_{max} obtained by fitting the raw data to the standard Michaelis-Menten equation are 27.0±2.3 μM and 7.7±0.15 umol/min/mg for untreated *cgl*-IDUA, and 77.0±12.0 μM and 3.6±0.18 umol/min/mg for deglycosylated *cgl*-IDUA.

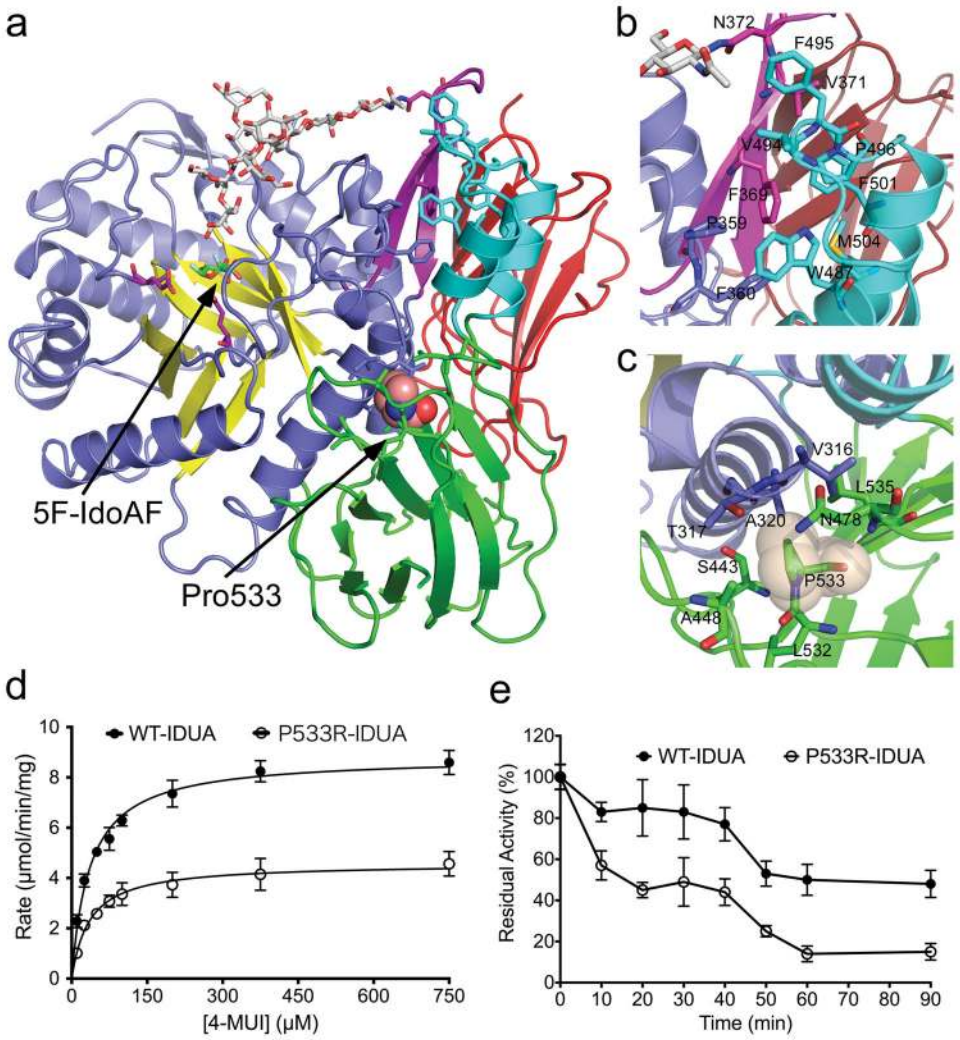

Figure 5. Structural and biochemical analyses of the Pro533Arg mutation in IDUA

(a) A full-molecule view of the Pro533Arg mutation relative to the active site, the Asn372-linked N-glycan, and the unique insertions in the IDUA protein (magenta, β23 and β24; cyan, α15 and α16). The domains of IDUA are colored as in Fig. 1. The Asn372-linked N-glycan and the bound 5F-IdoAF are represented as sticks with grey and green carbon atoms, respectively. Pro533 is shown as space-filling spheres with salmon-colored carbon atoms. **(b)** Hydrophobic packing among α15, α16, β23 and β24 contributes to stabilizing the conformation of the Asn372 N-glycan. **(c)** The side chain of Pro533 is involved in multiple van der Waals interactions with several nearby residues. **(d)** The Michaelis-Menten kinetics of the wild-type and Pro533Arg mutant enzymes. The assays were carried out in triplicates and results are presented as mean ± s.d.. The K_m and V_{max} values obtained by fitting the raw data to the standard Michaelis-Menten equation are 36.2±2.9 μM and 8.8±0.18 umol/min/mg for wild-type IDUA, and 35.3±3.66 μM and 4.5±0.15 umol/min/mg for the Pro533Arg mutant. **(e)** Time course of the effect of heat inactivation at 50 °C on the catalytic activities of the wild-type and the Pro533Arg mutant enzymes measured at 37 °C. For each enzyme, three samples were assayed at each time point and results are shown as mean ± s.d..

The level of decrease in enzyme activity is significantly greater ($p<0.05$) for the Pro533Arg mutant in comparison with that for the wild-type enzyme.